1

Introduction of Varistor Ceramics

Zinc oxide (ZnO) varistor, which is a kind of polycrystalline semiconductor ceramic composed of multiple metal oxides and sintered using conventional ceramic technology, is a voltage-dependent switching device, which exhibits highly nonohmic current–voltage characteristics above the breakdown voltage. Basic information on ZnO varistors, including the fabrication, microstructure, and typical electrical parameters, is introduced. The history and applications of ZnO varistors are also presented. The panorama of alternative varistor ceramics for Bi_2O_3-based ZnO varistors is mapped out. Especially, the ceramic–polymer composite varistors with lower breakdown voltage, incorporating varistor particles such as semiconducting particles, a combination of metal and semiconducting particles, and ZnO microvaristors, in a polymeric matrix are reported. Now, varistors are available that can protect circuits over a very wide range of voltages, from a few volts for low voltage varistors in semiconductor circuits to 1000 kV AC and ±1100 kV DC in electrical power transmission and distribution networks. Correspondingly, they also can handle an enormous range of energies from a few joules to many megajoules.

1.1 ZnO Varistors

A varistor is an electronic component with a "diode-like" nonlinear current–voltage characteristic, which is a portmanteau of variable resistor [1]. Functionally, varistors are equivalent to a back-to-back Zener diode and are typically used in parallel with circuits to protect them against excessive transient voltages in such a way that, when triggered, they will shunt the current created by the high voltage away from sensitive components.

The most common type of varistor is the metal oxide varistor (MOV), which contains a ceramic mass of ZnO grains, in a matrix of other metal oxides, such as small amounts of bismuth, cobalt, and manganese, sandwiched between two metal electrodes. The boundary between each grain and its neighbor controls the current according to the applied voltage, and allows current to flow in two directions. The mass of randomly oriented grains is electrically equivalent to a network of back-to-back diode pairs, each pair in parallel with many other pairs. A varistor's function is to conduct significantly increased current when voltage is excessive. Only nonohmic variable resistors are usually called varistors [1].

Metal Oxide Varistors: From Microstructure to Macro-Characteristics, First Edition. Jinliang He.

In normal use, a varistor is subject to a voltage below its characteristic breakdown voltage and passes only a tiny leakage current. When the voltage exceeds the breakdown voltage, the varistor becomes highly conducting and draws a large current through it, usually to ground. When the voltage returns to normal, the varistor returns to its high-resistance state [2]. The result of this behavior is a highly nonlinear current–voltage characteristic [3–5], in which the MOV has a high resistance at low voltages and a low resistance at high voltages; usually, the resistivity of a ZnO varistor is more than 10^{10} Ω cm below the breakdown voltage, whereas it is less than several ohm-centimeters above the breakdown voltage [6]. The switch is reversible with little or no hysteresis although it can degrade under electrical loading [2]. A varistor remains nonconductive as a shunt-mode device during normal operation when the voltage across it remains well below its "clamping voltage"; thus varistors are typically used for suppressing line voltage surges. However, a varistor may not be able to successfully limit a very large surge from an event such as a lightning strike where the energy involved is many orders of magnitude greater than it can handle. Follow-through current resulting from a strike may generate excessive current that completely destroys the varistor [1].

ZnO varistors are voltage-dependent switching devices, which exhibit highly nonohmic current–voltage (I–V) characteristics above the breakdown voltage. The nonohmic I–V characteristics are usually expressed logarithmically, as shown in Figure 1.1 [6]. The degree of nonohmic property is usually expressed by a nonlinear coefficient α defined by the following equation:

$$\alpha = \frac{V}{I}\frac{\mathrm{d}V}{\mathrm{d}I} \tag{1.1}$$

Empirically, the following simple equation is used:

$$I = \left(\frac{V}{C}\right)^{\alpha} \tag{1.2}$$

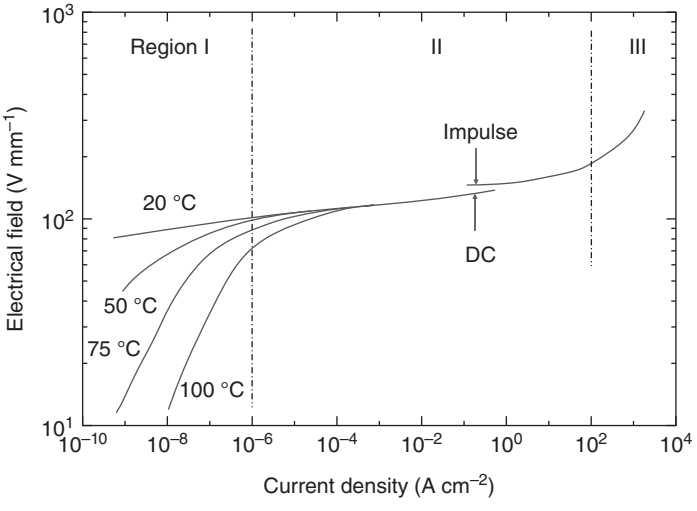

Figure 1.1 *I–V* characteristics of a typical ZnO varistor. Source: Adapted from Eda [6].

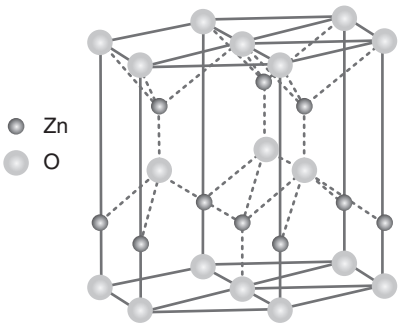

Figure 1.2 The wurtzite structure of ZnO. Source: Adapted from Addison [7].

where C is a constant. Typical α values of ZnO varistors are from 30 to 100; therefore, the current varies by orders of magnitude with only small changes in voltage. A more accurate measure of the nonlinearity is the dynamic conductance, the differential of the characteristic, at each voltage [2]. On the contrary, α values of conventional varistors such as SiC varistors do not exceed 10.

The I–V characteristics of ZnO varistors are classified into three regions, as shown in Figure 1.2 [6]. In region I (low electrical field region, or pre-breakdown region), below the breakdown voltage (typically a voltage at 1 μA cm^{-2}), the nonohmic property is not so prominent and can be regarded as ohmic, and the leakage current is highly temperature dependent. In region II (medium electrical field region, nonlinear region, or breakdown region), between the breakdown voltage and a voltage at a current of about 100 A cm^{-2}, the nonohmic property is very prominent and almost independent of temperature. In region III (high electrical field region or upturn region), above 100 A cm^{-2}, the nonohmic property gradually decays, and the varistor is again ohmic. These three regions in engineering applications are also called as the low current region, medium current region, and high current region, respectively.

ZnO varistors are characterized by the magnitude of the α values and the width of the range where highly nonohmic property is exhibited. In contrast to the pre-breakdown region, the nonlinear region and upturn region are little affected by temperature. The I–V characteristics below 100 mA cm^{-2} are usually measured using a DC electric source, whereas those above 1 A cm^{-2} are measured by an impulse current source to avoid heat generation and thermal breakdown. The waveform of the impulse current is 8/20 μs with an 8 μs rise time and 20 μs decay time up to one-half the peak value [6], which is used as a standard impulse current to test ZnO varistors. The I–V characteristics measured by the impulse currents show voltages higher than those measured using DC. The discrepancy is usually 10–20%, as shown by arrows in Figure 1.1 [6]. This discrepancy is caused by the delay in electrical response in the ZnO varistors. The response delay is speculated to be caused by electron trapping and hole creation at the grain boundaries.

1.2 Fabrication of ZnO Varistors

ZnO has a wurtzite structure in which the oxygen atoms are arranged in a hexagonal close-packed type of lattice with zinc atoms occupying half the

tetrahedral sites, as shown in Figure 1.2; Zn and O atoms are tetrahedrally coordinated to each other and are equivalent in position. The ZnO structure is thus relatively open with all the octahedral and half the tetrahedral sites empty. It is, therefore, relatively easy to incorporate external dopants into the ZnO lattice. The open structure also has a bearing on the nature of defects and the mechanism of diffusion, and the most common defect in ZnO is the metal in the open interstitial sites [8]. Pure ZnO without any impurities or dopants is a nonstoichiometric n-type semiconductor with linear or ohmic behavior, and with a wide band gap (3.437 eV at 2 K) [8, 9].

ZnO varistors are semiconducting ceramics fabricated by sintering of ZnO powders with small amounts of various metal oxide additives such as Bi_2O_3, CoO, MnO, and Sb_2O_3. The nonohmic property comes from grain boundaries between semiconducting ZnO grains. These oxides are added to control one or more of the properties such as the electrical characteristics (breakdown voltage, non-linearity, and leakage current), grain growth, or the sintering process [10–18]. Bi_2O_3 is the most essential component for forming the nonohmic behavior, and addition of CoO and MnO enhances the nonlinear properties [11, 12, 19–22]. A very low concentration of Al_2O_3 increases the ZnO grain conductivity while Sb_2O_3 controls the ZnO grain growth [23–32]. Combination of additives such as Cr_2O_3, MnO, Bi_2O_3, and CoO produces greater nonlinearity than a single dopant [10]. During high temperature sintering different phases are formed and the microstructure of a ZnO varistor comprises conductive ZnO grains surrounded by electrically insulating grain boundary regions.

Dopants play at least three major roles in forming varistors by affecting grain growth during sintering, the dewetting characteristics of the liquid phase during cooling, and the electronic defect states that control the overall varistor characteristics [2]. In order to obtain high performance ZnO varistors, the compositions, impurities, mixing methods, particle sizes, and sintering conditions, such as maximum temperature and holding time, temperature rising/lowering rates, and oxygen and Bi_2O_3 partial pressures, should be controlled precisely. This will be discussed in detail in Chapter 3.

1.2.1 Preparation of Raw Materials

ZnO varistors are commonly produced by conventional ceramic technology. The preparation process of ZnO varistors is basically the same as for general ceramics, whose primary processes include raw materials preparation, mixing, stoving and sieving, pre-sintering, smashing, prilling, molding, sintering, silvering, and testing. The preparation begins with weighing, mixing, and milling of oxide powders in ball mills. After the addition of organic binder substances, the aqueous slurry is spray-dried to produce a granulate. After sieving appropriate fractions to extract dust and large agglomerated particles, the material is transferred to hydraulic pressing machines to mold the "green" disks [33]. In the whole process, raw materials preparation and sintering are the two key steps that determine the electrical properties of ZnO varistors.

The preparation of material powders of ZnO varistors actually involves two steps: the preparation of ZnO powder and the mixing of ZnO powder with other additives. Usually, both steps are often combined as an inseparable one, so as to

achieve a one-step preparation of composite raw powders of the ZnO varistor ceramics.

The preparation of pure ZnO powder is divided into three traditional methods:

- *Direct method:* Zinc powder is added to reducing agents such as coke and coal, and heated at a high temperature to form reduced Zn steam, and then oxidized to ZnO by air.
- *Indirect method:* the zinc ingots are melted into the hot crucible to evaporate, so as to form the Zn steam, and then oxidized to ZnO by air.
- *Wet method:* The $ZnSO_4$ or Zn salt solution such as $ZnCl_2$ reacts with the Na_2CO_3 solution to crystallize the $ZnCO_3$ precipitation, and ZnO is generated by washing and filtering and heating to decompose the sediment.

In order to prepare high quality ZnO powder, some liquid- and gas-phase methods have been also used for the preparation of ZnO powders alone.

There are many ways of preparing ZnO varistor ceramic composite powders. According to the material states, the methods can be summarized as the solid phase, liquid phase, and gas phase one.

- *Solid-phase method:* it applies for the uniform mixing of ZnO solid powder and solid powder of other additives by mechanical milling. This is the conventional method used in the industry. However, it is difficult to obtain powders with uniform particle size distribution through this process.
- *Liquid-phase method:* it is developed from the wet method in the pure ZnO powder preparation. In liquid-phase synthesis, as components are fully dispersed in the liquid phase the content of each component can be precisely controlled. The solid-phase grain size produced is small with narrow size distribution, and particles of spherical or nearly spherical shape are obtained. The liquid-phase method is now becoming more and more common in the ZnO varistor ceramics industry, and it includes precipitation calcination, sol–gel, spray pyrolysis, hydrothermal method, and so on.
- *Gas phase method:* this method includes chemical vapor oxidation, laser heating, and so on. But the gas-phase method is of high cost, and it is difficult to achieve mass production using this.

Combustion synthesis technique was also used to successfully produce pure and doped pure crystalline ZnO varistor powders with good compositional control. The combustion synthesis route enables synthesis at low temperatures and the products obtained are in a finely divided state with large surface areas. Combustion synthesis offers as added advantages, the simplicity of experimental setup, the surprisingly short time between the preparation of reactants and the availability of the final product, the savings in external energy consumption, and the equally important potential of simplifying the processing prior to forming, providing a simple alternative to other more elaborate techniques [34].

1.2.2 Sintering of ZnO Varistors

ZnO varistor is fabricated by the traditional ceramic sintering technology, and the temperature control of the sintering process has a critical influence on the performances of the final products. The sintering procedure includes warm-up,

constant-temperature, and cooling periods. The pressed disks are sintered in an electric furnace at 1150–1350 °C for one to five hours in air, and the temperature is increased or decreased at 50–200 °C h^{-1}. During the warm-up and constant-temperature periods several chemical phase transformations take place, which result in a complete rearrangement of the microscopic particles and the creation of a dense polycrystalline matrix of ZnO grains and other phases, which are incorporated therein. The homogeneity of the ceramic microstructure strongly depends on the initial distribution of the reacting particles in the green body, and inhomogeneously distributed additives can result in islands of exaggerated or hampered ZnO grain growth or porosity, while such defects lead to bad electrical performance [33]. Finally, electrodes are prepared on both surfaces. The best electrodes are painted In–Ga alloys or evaporated Al films. Conventional silver electrodes painted and fired at 500–800 °C are also used [6].

The solid-state-based ceramic processing route still remains the preferred method of manufacturing because of the simplicity, cost, and availability of the metal oxide additives; this process has considerable disadvantages especially for many modern commercial applications. A major disadvantage of this route is the difficulty in obtaining additive homogeneity at a microscopic level, which is especially important for the manufacture of miniaturized electronic equipment. Processing methods and additive homogeneity are the critical parameters to produce a varistor material with favorable electrical characteristics. Inhomogeneous microstructures could cause degradation of varistors during electrical operation. Therefore, careful control of the microstructure is required to produce a varistor of desired characteristics [10].

Chemical processing, such as sol–gel, solution, precipitation, and microemulsion techniques, facilitates homogeneous doping at the molecular level. Among those various methods reported, sol–gel processing is found to be a promising one to obtain a miniature device with higher breakdown voltage, low leakage current, and reasonably good nonlinear characteristics [10]. However, controlling the grain growth at high sintering temperatures still remains a challenge for varistor ceramics, and the electrical properties could be improved if the materials could be sintered to full density with sub-micrometer or nanometer grain size. Researchers have proposed seed law method, stacking method, hot pressing method, microwave sintering method, and other technologies for the sintering of ZnO varistor ceramics [6]. Indeed, a significant enhancement in electrical properties has been achieved by novel sintering procedures such as step sintering, spark plasma sintering, or using microwave irradiation [10]. This will be introduced in Chapter 9.

1.3 Microstructure

Conventional varistors are usually prepared by mixing 0.2–1 μm sized ZnO powders with oxide additives. Although the microstructures of varistors exhibit considerable variation from one manufacturer to another, they all exhibit the characteristics of a typical ceramic prepared by liquid-phase sintering. ZnO

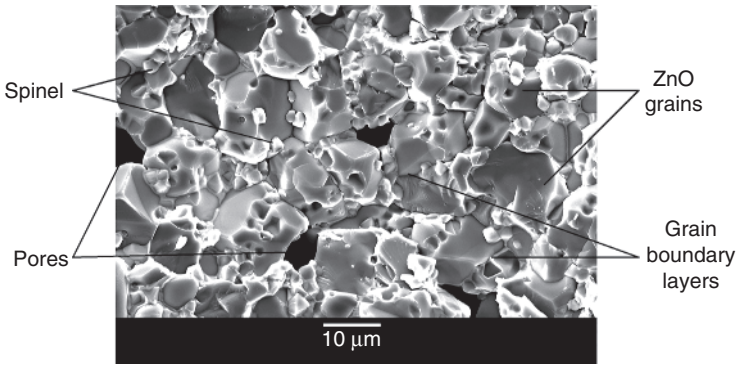

Figure 1.3 SEM photomicrograph of ZnO varistor microstructure.

varistors are polycrystalline materials composed of semiconducting ZnO grains with their attendant grain boundaries as shown in Figure 1.3. Moreover, the microstructure contains particles of one or more types of spinel, and a lot of remaining pores can be primarily found in the grain boundaries. Depending on the composition, twins within the ZnO grains and a small amount of a pyrochlore phase can also form. The ZnO–Bi_2O_3–Sb_2O_3 system forms a pyrochlore phase $Zn_2Bi_3Sb_3O_{14}$ above 650 °C. With ZnO, pyrochlore further reacts to form a spinel ($Zn_7Sb_2O_{12}$) [12, 35].

The grain boundary has a relatively thick (0.1–1 pm) Bi_2O_3-rich intergranular layer, which becomes thinner (10–1000 Å) as it approaches the contact points of the particles [6]. The sizes of ZnO grains are usually 5–20 μm and depend on the material composition, temperature, and time of sintering. The resistivity of a ZnO grain is 0.1–1 Ω cm. The grain boundaries are highly resistive and show nonohmic property, and the corresponding breakdown voltage is around 200–400 V mm^{-1} for conventional varistors, and the breakdown voltage per grain boundary is about 3 V. The breakdown voltage of the sintered body is proportional to the number of grain boundaries between the two electrodes. This indicates that the breakdown voltage is proportional to the inverse of the ZnO grain size [6].

The characteristics of ZnO varistor ceramics are closely related to their microstructure, which is characterized by the following parameters: ZnO grain size and the grain size distribution, grain boundaries, secondary phases such as the Bi_2O_3-rich phase, $Zn_7Sb_2O_{12}$ spinel-type phase, and $Bi_3Zn_2Sb_3O_{14}$ pyrochlore-type phase, the distribution of secondary phases along the grain boundaries, and the size and distribution of pores [36].

1.4 Typical Parameters of ZnO Varistors

The nonlinear voltage–current (V–I) characteristics of ZnO varistors can be approximately expressed by Eq. (1.2). In Figure 1.4 [37], the V–I nonlinear curve is shown, where the bi-logarithm coordinates are used, and the voltage and current are represented by the voltage gradient and current density, respectively.

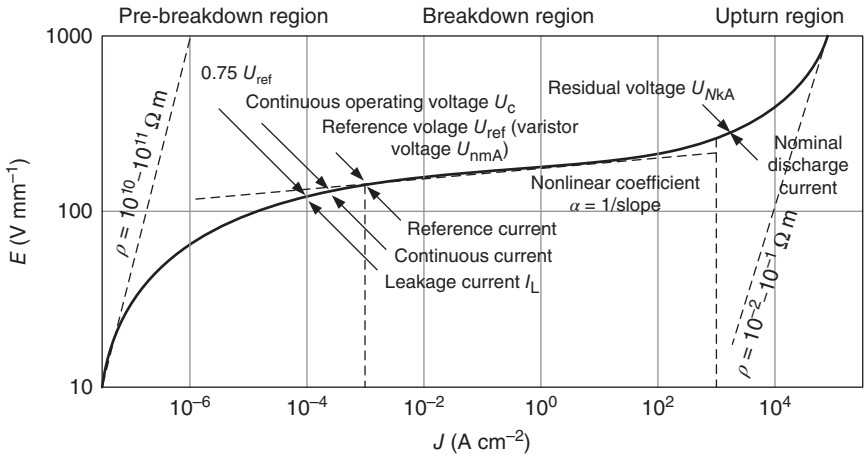

Figure 1.4 Nonlinear voltage–current (*V–I*) characteristics of ZnO varistors.

The nonlinear $V–I$ characteristics of ZnO varistors is mainly indicated by the following parameters, some of which only apply to the high voltage electrical applications [37].

Nonlinear coefficient α: it represents the reciprocal of the slope of the straight part in the $V–I$ curve, and generally refers to the corresponding value of the breakdown region. The larger the value is, the better the performance.

Varistor voltage $U_{n\mathrm{mA}}$: it refers to the voltage of the varistor at the turning point of the curve, at a specific value of current (between 0.1 and several milliamperes, usually 1 mA), also called the reference voltage. For the convenience of performance comparison, it is usually represented by the voltage gradient $E_{n\mathrm{mA}}$:

$$E_{n\mathrm{mA}} = \frac{U_{n\mathrm{mA}}}{d} \tag{1.3}$$

where d is the thickness of the varistor disk.

Chargeability (or voltage undertaking ratio) S: it is defined by the ratio of the crest value of the continuous operating voltage to the varistor voltage $U_{n\mathrm{mA}}$; it represents the load voltage intensity at continuous operation condition.

Leakage current I_{L}: refers to the current flowing through the varistor at the set temperature and voltage, which is less than the varistor voltage, and usually takes 0.75 $U_{1\mathrm{mA}}$ as the test condition.

Residual voltage $U_{N\mathrm{kA}}$: it refers to the impulse voltage occurring at the set impulse current of N kA. In high voltage applications, it is usually represented by impulse current residual voltage, lightning current residual voltage, and steep-wave current residual voltage.

Residual voltage ratio K: it refers to the ratio of the residual voltage to the varistor voltage, namely, $U_{N\mathrm{kA}}/U_{n\mathrm{mA}}$.

Discharge capacity: it refers to the maximum impulse current value allowed to flow through the varistor in the set conditions, including a 2 ms square wave and a 4/10 μs impulse current.

Energy absorption capability (or energy handling capability) is the second most important property of ZnO varistors next to nonlinearity. ZnO varistors as the core elements of surge arresters in high voltage systems or surge protection devices (SPDs) in low voltage systems are required to absorb substantial amounts of energy resulting from temporary overvoltages, switching surges, or lightning impulses. Therefore, the energy absorption capabilities of ZnO varistors are crucial for the integrity of equipment and systems. However, it has been observed in experiments that differences in barrier voltages, grain sizes, and grain boundary characteristics inside the same ZnO varistor and among different ZnO varistors cause nonuniformity in the microstructurally electrical and thermophysical characteristics of ZnO varistors, and finally result in the differences in their current handling capabilities, which is also called as the energy absorption capability and has a direct relation to the failure modes. Failure modes include electrical puncture, physical cracking, and thermal runaway, which happen under different currents. The energy absorption capability can be divided into thermal energy absorption capability and impulse energy absorption capability. For the impulse energy absorption capability single impulse stress, multiple impulse stress (without sufficient cooling between the impulses), and repeated impulse stress (with sufficient cooling between the stresses) have to be considered. Thermal energy absorption capability, on the other hand, can only be considered for complete metal oxide arresters (MOAs) or SPDs, as it is mainly affected by the heat dissipation capability of the overall arrester design, besides the electrical properties of the MOVs.

Another important electrical characteristic of ZnO varistors is the dielectric property. Below the breakdown voltage, ZnO varistors are highly capacitive. The dielectric constant of ZnO is 8.5, whereas an apparent dielectric constant of a ZnO varistor is typically 1000. The dielectric properties are mainly caused by thin depletion layers (~1000 Å) at the grain boundaries [6].

1.5 History of ZnO Varistors

The ZnO varistors were first developed by Matsuoka and his research group at Matsushita Electric (Japan) in 1969 [38] and were commercialized under the trade name ZNR in the following year [6]. In 1979, they introduced many of the essential features of ZnO varistors as we know them today in detail [3], which included making ZnO semiconducting by adding substitutional ions, densification by liquid-phase sintering with a Bi_2O_3-rich liquid phase, segregation of large ions to the grain boundaries, and the main formulas with high nonlinearity by doping manganese and cobalt. Although work on the electrical properties of ZnO ceramics apparently had been underway in Russia in the early 1950s [39, 40], it was Matsuoka's work [3] that captured attention, and, shortly thereafter, a joint development effort was undertaken by GE and Matsushita [41]; one of Matsuoka's contributions was the discovery of the role of aluminum [42]. It was in the period following this that extensive literature was documented and the scientific basis for varistors as well as many of the

key technological developments was established. Concurrently, the superiority of ZnO varistors over SiC varistors for many applications was established, and expertise in utilizing ZnO varistors spread geographically. More companies began to manufacture varistors, and alternative sets of dopants were introduced, but the essential features introduced by Matsuoka remained [2]. The one exception was the use of Pr_2O_3 in the place of Bi_2O_3 [43, 44].

The performance parameters of ZnO are closely related to the raw formulas. By changing the percentage and compositions of the additives, the performance of ZnO varistors changes correspondingly. According to the additives, industrial ZnO varistors are mainly divided into two series:

- The ZnO–Bi_2O_3 series, or Bi-series, mainly includes additives such as Bi_2O_3, Sb_2O_3, Co_2O_3, MnO_2, and Cr_2O_3 [3];
- The ZnO–Pr_2O_3/Pr_6O_{11} series, or Pr-series, mainly includes additives such as Pr_2O_3/Pr_6O_{11}, Co_2O_3, and CaO [43, 44].

Many efficient additives were discovered. Eda [6] and Gupta [8] separately summarized and classified the additives into four types according to their effects:

- Additives such as Bi_2O_3, Pr_2O_3, BaO, SrO, and PbO, which make ZnO form a grain boundary structure, mainly promote liquid-phase sintering to form grain boundaries and make the materials nonlinear.
- Additives such as Co_2O_3, MnO_2, Sb_2O_3, Al_2O_3, and Ga_2O_3 improve the nonlinearity of the ZnO varistor. Part of these additives solidly solutes in ZnO grains to form impurity traps to provide carriers as donors, while the others form traps to promote the barrier height as acceptors.
- Additives such as Sb_2O_3, SiO_2, and TiO_2 affect the growth of ZnO grains by promotion or inhibition; the size of ZnO grains can be controlled, and the voltage gradient is tailored.
- Additives such as Sb_2O_3, SiO_2, NiO, and frit mainly improve the stability of ZnO varistors.

In the first decade after the Matsuoka's invention, various additives to improve the electrical characteristics were discovered and the processing conditions were optimized. This will be introduced in Chapter 3. In the next decade, the microstructures and the physical properties of the grain boundaries were gradually identified, and applications were rapidly found in protecting electrical equipment and electronic components such as transistors and integrated circuits (ICs) against voltage surges [6].

Many efforts have been made in the past several decades focusing on the conduction mechanism in the ZnO varistor; among the numerous conduction models proposed by different research groups, the one presented by Pike [45, 46] and further developed by Blatter and Greuter [47–49] has been widely recognized and may meet most of the experimental phenomena. Essentially, it is believed that the nonlinear V–I characteristic of the ZnO varistor is caused by the charge carriers transporting across the double Schottky barrier (DSB) formed at the grain boundary. The conduction mechanism of the ZnO varistor will be introduced in Chapter 2.

The electrical properties of each individual grain boundary will contribute to the global electrical characteristics of ZnO varistors. By microcontact electrical measurements on multiple-phase ZnO varistors, the grain boundaries were simply classified into good, bad, and ohmic ones according to the electrical characteristics of grain boundaries, and a high percentage of grain boundaries had bad or ohmic $I–V$ characteristics, and only a small percentage of grain boundaries had good $I–V$ characteristics. These few good grain boundaries are responsible for the good varistor effect and control the leakage current of the ZnO varistor at low values of applied voltage [50]. So, it is very important to understand the influence of the junction network on the device properties [51]. The microstructural electrical characteristics of ZnO varistors will be introduced in Chapter 4.

The influence of the geometry and topology of the granular microstructure as well as the properties and the distribution of electrical characteristics of grain boundaries on the features of bulk varistor devices is another important issue. The simulation study of such systems is helpful to reveal the connection between the microstructure and macroscopic characteristics of varistor ceramics. This was recognized early in the development of ZnO varistors, and a number of consequences were discussed based on the idea that the disorder resulted in "chains" of more conducting paths through the microstructure [2]. One of the most important simulation models is where Bartkowiak and Mahan [52] used the Voronoi network to present the actual microstructures of ZnO varistors with randomly distributed ZnO grains and grain boundaries. The details on how to simulate varistor ceramics will be introduced in Chapter 5.

The breakdown of ZnO varistors is an original phenomenon during their application, which has been reported in many publications [53–60]. It has been found that every varistor has a different destruction phenomenon under impulse current and AC or DC current. Three failure modes have been identified [61]: electrical puncture, physical cracking, and thermal runaway (or thermal breakdown); these failure models result in different energy handling capabilities. This will be introduced in Chapter 6.

ZnO varistors can be electrically, chemically, and thermally degraded during use, leading to a reduction in barrier voltage height and, consequently, an increase in leakage current, which could be catastrophic for ZnO varistors. In the past few decades, much research has been carried out to explain the observed degradation phenomena of ZnO varistors, and correspondingly various degradation mechanisms of grain boundaries have been proposed, e.g. electron trapping, dipole orientation, ion migration, and oxygen desorption [62–64]. Among these mechanisms, ion migration has found comparatively strong support on the basis of different circumstantial evidences. Electrical degradation of ZnO varistors will be introduced in Chapter 7.

Processing for increased reliability, microstructural uniformity, and resistance to degradation has continued to the present and has also become more sophisticated through the use of improvements in process control, chemical routes to homogenization of powders, and even formulation optimization through techniques such as neural network modeling [2].

Now, varistors are available that can protect circuits over a very wide range of voltages, from a few volts for low-voltage varistors in semiconductor circuits to

11 000 kV AC and ±1100 kV DC in electrical power transmission and distribution networks. Correspondingly, they can also handle an enormous range of energies from a few joules to many megajoules. Remarkably, they are also very fast, switching within nanoseconds from their high resistance state to a highly conducting state [2].

1.6 Applications of ZnO Varistors

MOV, which is also called as ZnO varistor, has good nonlinear volt–ampere characteristics and excellent impulse energy absorbing capacity; these advantages enable wide MOV usage in transient overvoltage protection for electrical/electronic systems. In low voltage systems, MOV, shown in Figure 1.5a, is assembled as SPDs as in Figure 1.5b; in high voltage fields, MOVs, which have disk shape or ring shape as shown in Figure 1.6a, are manufactured as surge arresters as in Figure 1.6b; MOVs are also used as energy absorbing devices in electrical/electronic systems. Surge arresters are devices that help prevent

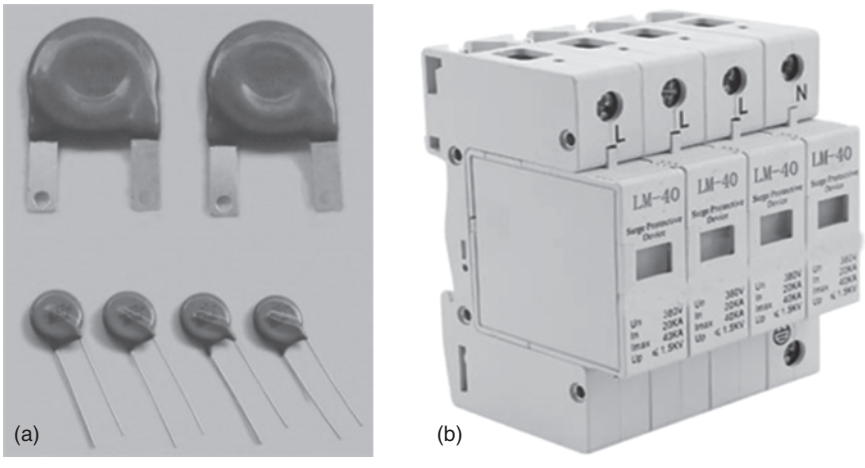

Figure 1.5 (a) Metal oxide varistors for low voltage systems and (b) surge protection devices (SPDs).

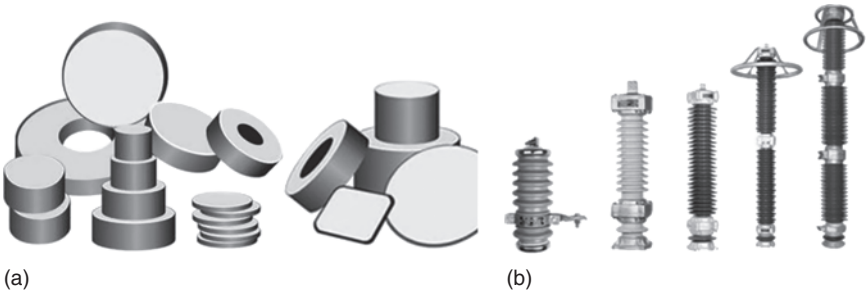

Figure 1.6 (a) Metal oxide varistors for high voltage systems and (b) surge arresters with porcelain houses.

damage to apparatus due to high voltages. The arrester provides a low-impedance path to ground for the current from a lightning strike or transient voltage and then restores to normal high-impedance operating conditions.

The surge arrester is the key overvoltage protection equipment in electrical power systems, and the insulation level of power apparatus is determined by the overvoltage protection level of surge arresters. Lightning overvoltages were causing problems on overhead lines well before Tesla and Edison argued over the merits of AC and DC. Many of the overvoltage protection methods for distribution lines follow the same philosophy as that used for telegraph and telephone lines. For example, early surge protective devices on single-phase power lines used single or multiple air gaps, as shown in Figure 1.7 [65], which followed telegraph line protection measures closely. As shown in Figure 1.8, the development of surge arresters for transient overvoltage protection in power systems has experienced gap-type arrester, expulsion-type arrester, SiC valve-type arresters with internal spark gaps and magnetic blow gaps, and ZnO surge arresters. SiC varistor ceramics were developed in the early 1930s to replace early selenium rectifiers for protecting telephone systems. The materials developed by the Bell System consisted of partially sintered compacts of SiC particles [66, 67]. Successive improvements, particularly in processing, took

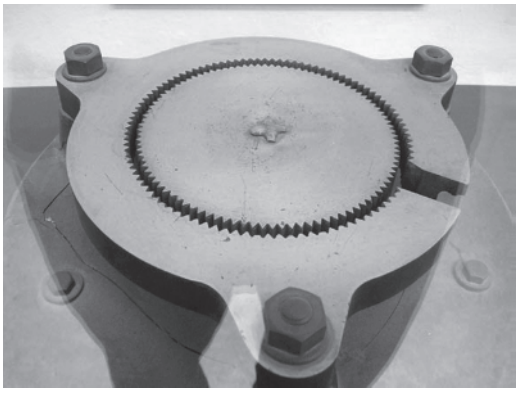

Figure 1.7 Lightning surge arrester, manufactured by Oerlikon in 1886 for Kriegstetten–Solothurn 2 kV power line. Source: Chisholm 2010 [65]. Reproduced with permission of IEEE.

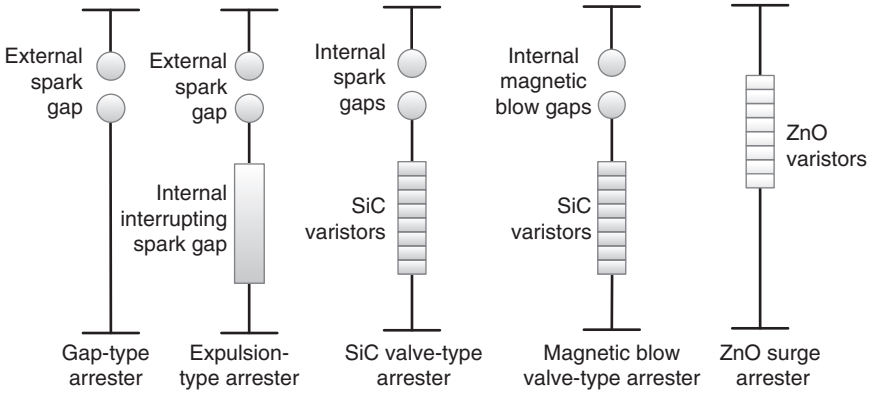

Figure 1.8 Technical development progress of surge arresters.

place both in the United States and in Japan [68]. The nonlinear coefficient of SiC varistors is less than 10, so the leakage current under operating voltage is too high and has to work with a series gap. But the ZnO varistor has high nonlinearity, and its leakage current under operating voltage is very small; usually ZnO surge arresters can work without a series gap, so ZnO surge arresters are of the gapless type. The ZnO surge arrester has good protection performance, quick response speed, and large energy handling capability; as a result, it has been widely accepted, popularized, and used in power systems. Figure 1.9 shows the application of surge arresters in 1000 kV ultrahigh voltage (UHV) AC substation.

The ZnO surge arresters used in Japan's UHV transmission systems were mainly developed by the Mitsubishi Corporation. Three kinds of ZnO varistors of different characteristics for UHV arresters, named as type A, B, and C, were manufactured. The volt–ampere characteristic of A-type varistor is similar to that of varistors used in the conventional 500 kV ZnO arresters. And B-type and C-type owned a more superior protection performance to meet the requirements of insulation of UHV systems, especially the C-type varistor. The C-type has the best performance and the lowest residual voltage, which makes it become the ultimate choice in UHV arresters in Japan [69].

The B-type arrester is used in 1000 kV systems whose rated voltage is 826 kV; when the 8/20 μs impulse current is 20 and 10 kA, the residual voltage is 1800 and 1710 kV, respectively, whereas the residual voltage of the C-type is only 1620 and 1550 kV when the current is 20 and 10 kA. Compared with the 1112 kV residual voltage with 20 kA current of the 500 kV arrester, the residual voltage

Figure 1.9 1000 kV ultrahigh voltage AC surge arresters with porcelain houses in Dongwu 1000 kV UHV AC substation. Source: Courtesy of X. Zhao.

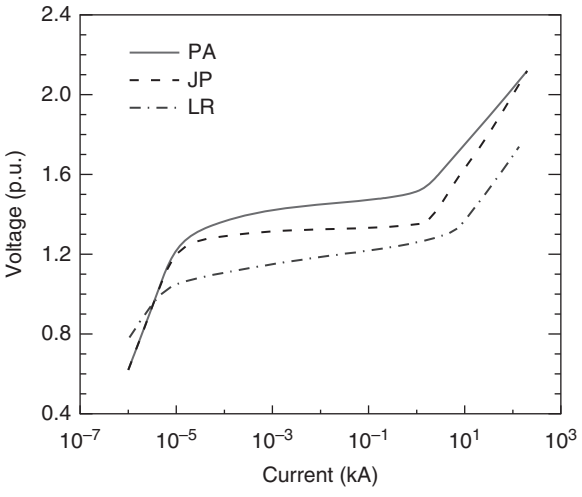

Figure 1.10 Volt–ampere characteristic curves of different UHV surge arresters: presently applied in China (PA), arrester used in Japan (JP), and low residual voltage arrester (LR), which is being developed in China. Source: He et al. 2011 [69]. Reproduced with permission of IEEE.

Figure 1.11 Ultrahigh voltage AC tank-type surge arresters in 1000 kV Jindongnan Substation in China.

of the C-type arrester increases by only 45.7% when the system voltage doubles. Figure 1.10 shows the data of volt–ampere characteristic curve of the C-type arrester used in Japanese UHV systems with a voltage base of 890 kV [69].

Except the ZnO surge arresters with porcelain houses, tank-type surge arresters in SF_6 insulation are widely used in gas-insulated substations (GISs); the 1000 kV UHV AC tank-type surge arresters, with height of 4455 mm and diameter of 2024 mm, are shown in Figure 1.11. Usually, ZnO surge arresters are assembled in porcelain houses, and applied in overvoltage protection in high voltage substations and distribution systems. Since the 1980s, ZnO surge arresters with polymeric houses have been developed, as shown in

Figure 1.12 Metal oxide surge arresters with polymeric houses.

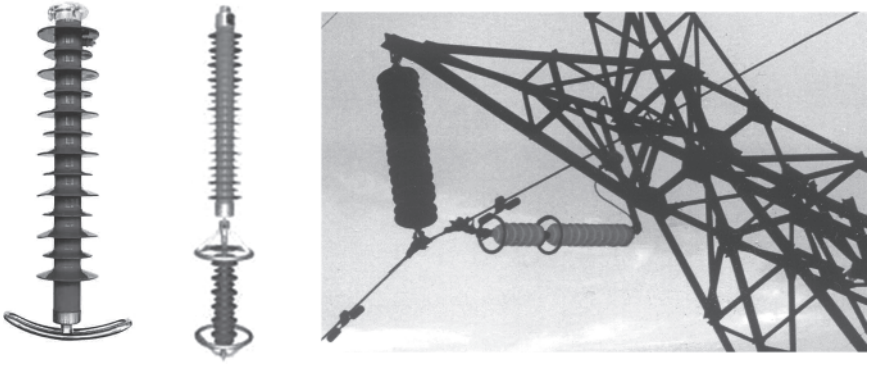

Figure 1.13 Line surge arresters and application on transmission line.

Figure 1.12. This kind of polymeric line surge arresters are very light, and have been applied in parallel with the insulators for lightning protection of high voltage transmission lines [70–77]. Typically, the polymeric line surge arrester has a whole-solid-insulation structure; all interior gaps are filled with middle temperature silicon rubber material. There is no gas gap inside the arrester [77]. We know that the main reason for porcelain house arrester failure is moisture ingress, so the failure of the whole-solid-insulation arrester caused by moisture ingress is eliminated. The polymeric housing not only makes the surge arrester smaller and lighter but also solves the problem of pressure relief due to the absence of air gap inside the polymeric arrester; the electrical, and therefore thermal, overloading of the ZnO varistors could not cause a flashover along the side surface of the ZnO varistor column. So the whole-solid-insulation polymeric surge arresters are of the safety type. Usually, the polymeric line surge arresters are assembled with series gaps as shown in Figure 1.13, and only

operate when lightning strikes the transmission line or the tower. It would not work under AC power frequency overvoltage or switching overvoltage, and keeps the state of "rest" due to the isolation of the series gap [77]. Now line surge arresters have been applied in 110–500 kV AC transmission lines, and ±500 kV to ±800 kV UHV DC transmission lines. The lightning protection performances of transmission lines have been highly improved due to the installation of these polymeric line surge arresters.

1.7 Alternative Varistor Ceramics

In order to overcome the shortcomings of Bi_2O_3-based ZnO varistors, other ZnO varistor systems have been added to ZnO varistors instead of bismuth, such as praseodymium [78, 79], barium [80], and vanadium [81]; all exhibit varistor behavior. All of them not only have a simple microstructure consisting of ZnO grain and intergranular layer, but also high nonlinearity. This will be introduced in Chapter 8.

Besides working to improve the performance of the ZnO varistor material, scientists are also searching for other new materials in order to achieve better stability and be used for new applications.

The integration of electronic circuitry into IC chips has brought large volume and weight reductions, so there is an increasing trend toward integration of passive electronic-ceramic components. In order to protect electronic circuits from damage due to surge voltages, the application of varistors within low voltage fields also rose. The titanium-based capacitor–varistor dual function varistor ceramics, such as TiO_2, $SrTiO_3$, and $CaCu_3Ti_4O_{12}$ (CCTO) varistors [82–88], have realized the goal of component miniaturization and provide superior high-frequency and high-amplitude transient voltage protection. This will be introduced in Chapter 10.

In 1995 [89], S.A. Pianaro found that SnO_2 varistor ceramics doped small amounts of additives obtained by solid-state sintering. Unlike the multiphase structure of ZnO-based varistor, SnO_2-based varistor has a simple microstructure and good stability. Dense SnO_2-based systems present values of nonlinear coefficient, breakdown voltage, and barrier voltage per grain equivalent to those of the traditional and commercial ZnO varistor [89–95], and better thermal conductivity; this makes SnO_2-based varistor one of the most promising candidates to compete commercially with ZnO-based varistor. SnO_2-based varistors will be introduced in Chapter 11.

WO_3-based varistor ceramic is another kind of low voltage varistor with a low threshold electric field of 5–10 V mm^{-1} and high dielectric constant [96–98]; this enables it to act as a varistor in parallel with a capacitor, which is attractive for applications in the elimination of electrical noise of micro-motors, protecting contact of delays, and absorbing discharges of some circuits. WO_3-based varistor ceramics will be introduced in Chapter 12.

More investigations have been carried out. The effect of CuO doping on the microstructure and electrical properties of Pr_6O_{11} varistors was investigated [99].

Minor CuO doping can improve the nonlinear electrical properties by offering more oxygen adsorption sites. Highly nonlinear current–voltage relations with voltage-limiting characteristics are observed for Mg-doped lanthanum calcium manganite polycrystalline ceramics with nonlinear coefficient of 2–9 at low electric field strengths of 2–5 V mm^{-1}, below magnetic transition temperatures [100]. The current density increases with external magnetic field, so that magnetically tunable low voltage varistors are realized.

Varistor action with a nonlinear coefficient of 3.9 and a breakdown voltage of 40 V mm^{-1} was observed in undoped terbium oxide ceramic and the sample exhibited excellent electrical stability up to 70 °C [101].

Not surprisingly, a number of polycrystalline semiconducting ferroelectrics also can be expected to exhibit varistor characteristics, albeit over a narrower range of temperature [102, 103].

1.8 Ceramic–Polymer Composite Varistors

Interestingly, the ceramic–polymer composite varistor is a composite one, incorporating varistor particles [104] or semiconducting particles, or a combination of metal and semiconducting particles, such as ZnO [105–107], SiC [108], and ZnO microvaristors in a polymeric matrix. The field-dependent property of the composites varies with filler concentration. When the filler concentration is above a critical value, which is called as percolation threshold, the composite begins to exhibit stable nonlinear properties, and current flows from one particle to the next through an interfacial region. Some studies concluded that for nonlinear composites with spherical fillers such as ZnO and SiC, high filler concentrations of typically 30–40 vol.% were required to obtain nonlinear electrical conductivity [109, 110].

The varistor particles themselves can exhibit nonlinear behavior, so the ceramic–polymer composite varistors exhibit nonlinearity in electrical conductivity [111–114] and function in a manner similar to the original incorporating varistor particles. Although the energy handling capabilities of composite varistors are generally inferior to those of solid ZnO varistors, their advantages in flexible shape and easy fabrication and formability make them attractive for many applications.

Composite varistors with lower breakdown voltage can be a suitable substitute for ZnO-based varistors for the purpose of protection of low voltage systems [114]. Low voltage varistors with good nonlinearity have been achieved using ZnO–polyaniline–polyvinyl alcohol (PVA) composites. Polymer composite thin films can be easily prepared by solution-casting technique. To increase the elasticity of final films and to prevent them from tearing PVA can be effectively employed in the varistor matrix. The devices with high nonlinearity coefficients (2.7–4.1) and low breakdown voltages (120–350 V) are useful in protecting sensitive electrical circuits [111–113]. The composite varistor with GaAs–polyaniline–polyethylene compositions can be easily prepared as thin disks using hot pressing method [111–113]. The samples with higher percentages

of GaAs (>50%) display varistor properties. They can be used to protect circuits from ~60 V up to over 90 V.

Silicon has some unique properties that make it important in the varistor industry [115]. The breakdown voltages of Si–polymer composite varistors were low in comparison with similar ZnO–polymer composite varistors [115, 116]. On the Si content exceeding 65% of the whole Si–polymer mixture, samples exhibited varistor behavior with a nonlinear coefficient of about 10. But at temperatures between 100 °C and 130 °C, the nonlinear conductivity of the varistor gradually turned to ohmic conductivity.

Polymer/perovskite manganese oxide (epoxy resin/$La_{0.8}Sr_{0.2}MnO_3$) composites were prepared using the bonded method [105]. There was no reaction between $La_{0.8}Sr_{0.2}MnO_3$ and the polymer. The nonlinear current–voltage property is significantly affected by the content of the polymer, and the nonlinear coefficient can exceed 45. The resistivity of the composites is five to nine orders of magnitude higher than that of the sintering ceramics.

In order to improve the nonlinearity of composite varistors, the ZnO microvaristor shown in Figure 1.14 [117], which was produced by the same fabrication technique and prescription of ZnO varistors, has been used as the filler in polymers [117–120]. ZnO microvaristor composites based on silicone matrix were prepared. The silicone and vulcanizing agent were mixed in 0.8 wt% with tetrahydrofuran solvent and blended by a high torque blender for about 20 minutes. After the silicone was fully dissolved in the solvent, ZnO microvaristor powders were poured into the liquor and the blending continued for 40 minutes. Then the mixture was dried in a vacuum oven for more than 10 hours till the solvents fully volatilized. This was followed by the process of vulcanization. Each time, a 3 g mixture was pressed by the vulcanizing machine at a pressure of 15 MPa at 170 °C for 15 minutes and then naturally cooled to room temperature at the same pressure. The acquired silicone rubber composite sample is about 0.5 mm in thickness and 20 mm in diameter.

Figure 1.15 presents the scanning electron microscopy (SEM) images of the ZnO microvaristor silicone rubber composites [117]; it is evident that many fillers

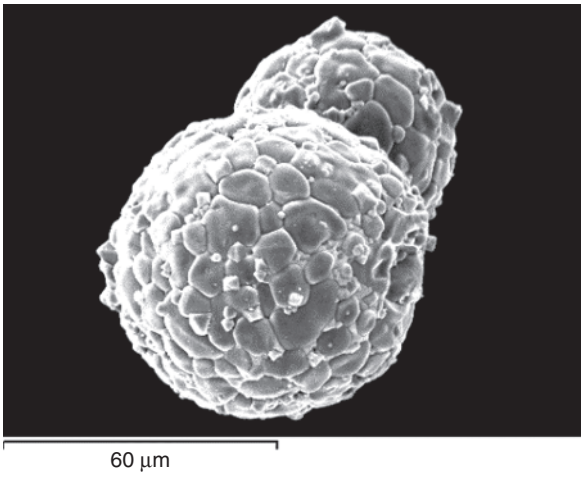

Figure 1.14 SEM image of two contacted ZnO microspherical varistors [117]. Source: https://creativecommons.org/licenses/by/4.0/.

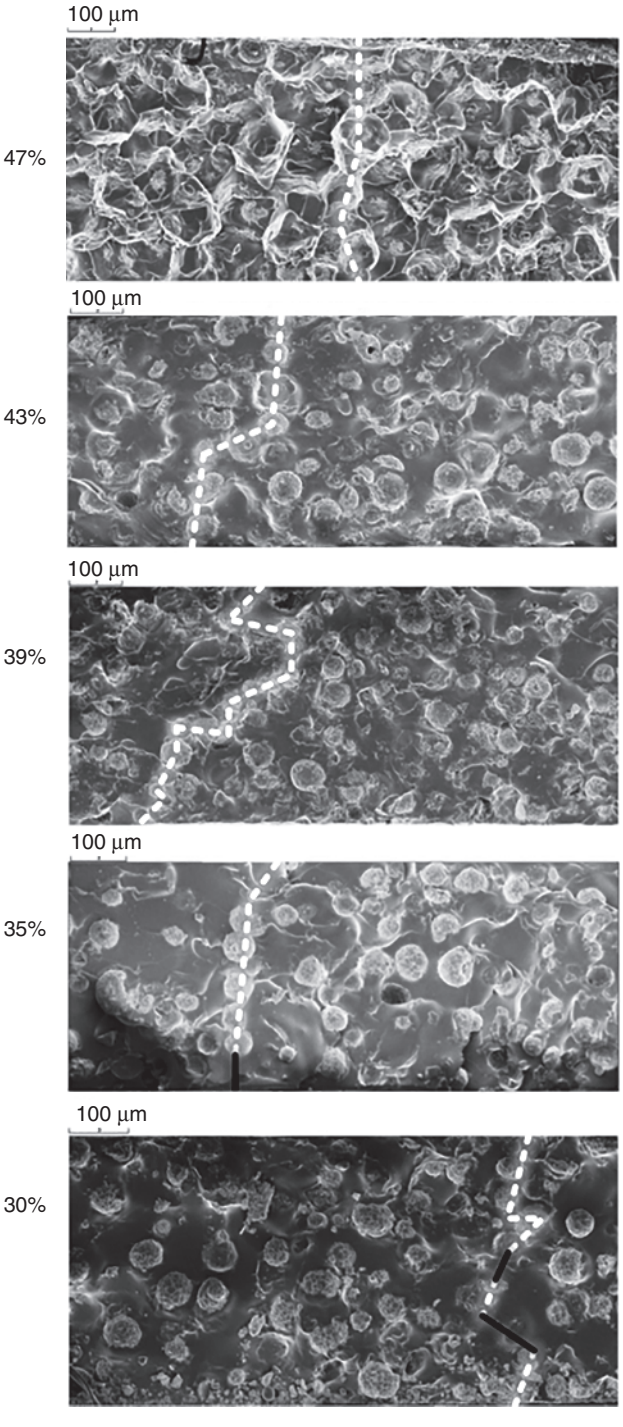

Figure 1.15 SEM images and possible conduction paths in ZnO microvaristor composites [117]. Source: https://creativecommons.org/licenses/by/4.0/.

are aligning in series. The conduction paths could be approximately determined and marked by the dotted lines. The solid lines indicate silicone rubber layers separating two adjacent fillers in a potential breakdown path. When the filler concentration is higher than the percolation threshold, which is 33%, in those samples, fillers form thoroughly connecting paths and the current selects the shortest one to flow through. It is evident that in composites with higher filler concentrations, a short conduction path is more likely to form, which means a lower switching field. The conduction paths become more and more straightforward from the 39% to 47% samples. As a result, the switching field decreases with filler concentration.

The nonlinear V–I characteristics of ZnO microvaristor/silicone rubber composites with different filler concentrations are shown in Figure 1.16 [117]. For the samples with filler volume concentrations of 39%, 43%, and 47%, the breakdown electric fields are almost the same and they decrease with increase in filler concentration. Samples with the above three filler concentrations present typical nonlinear behavior and can be attributed to the fully percolated case. For the 35% sample, the switching field is even higher and it exhibits the breakdown feature. This is a sign of approaching percolation. The switching field E_b and the nonlinear coefficient α are in the range from 330 to 826 V mm^{-1}, and from 10.2 to 17.5, respectively, with the filler's diameter ranging from 50 to 150 μm. Simulation results show good agreement with experimental ones.

ZnO microvaristor-filled related polymers, such as ZnO–epoxy [121], ZnO–LDPE (low-density polyethylene) [122], ZnO–LLDPE (linear low-density polyethylene) [118], and ZnO–polyester [107], were reported to possess different nonlinear characteristics with switching fields in the range of about

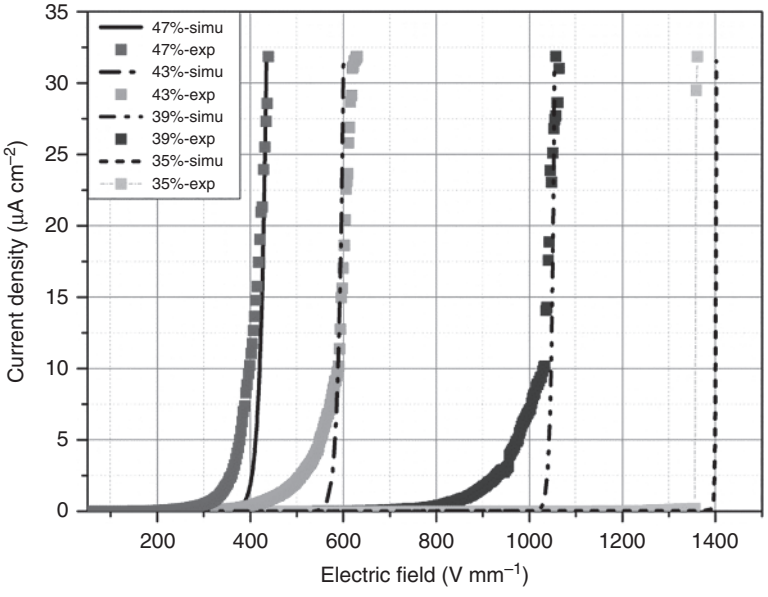

Figure 1.16 Nonlinear V–I characteristics of ZnO microvaristor composites with filler concentrations of 35%, 39%, 43%, and 47% [117]. Source: https://creativecommons.org/licenses/by/4.0/.

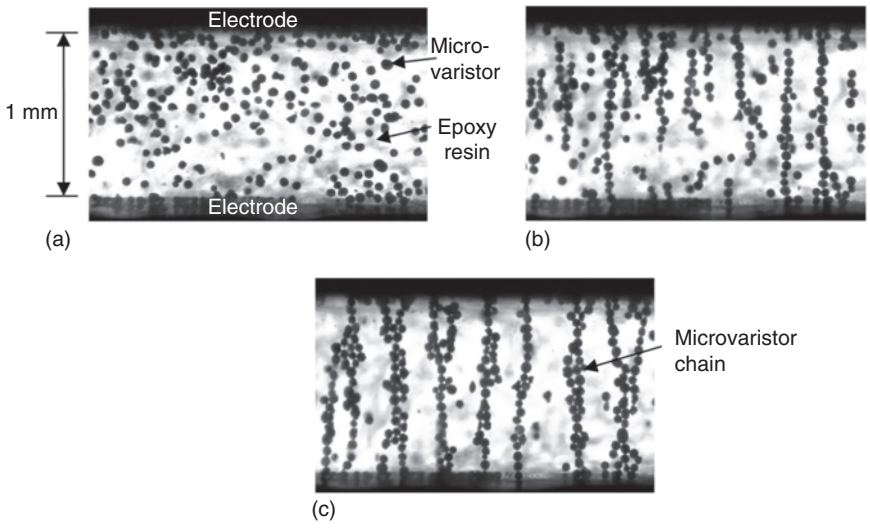

Figure 1.17 Behavior of microvaristors in an epoxy resin by field application. The microvaristor content is 20 wt%, and the applied field is 450 V_{rms} mm^{-1}. (a) Before field application; (b) 9 seconds after field application; (c) 65 seconds after field application. Source: Ishibe et al. 2014 [123]. Reproduced with permission of IEEE.

300–1000 V mm^{-1} and nonlinearity above 9. The difference is mainly due to the nature of the grain parameters such as grain size and preparing formula inside each microvaristor. Even so, all of the above ZnO composites present a similar pattern that the nonlinear conducting behavior varies with filler concentration. The switching field decreases with incremental filler concentration above the percolation threshold while the nonlinear coefficient remains stable. Under the threshold, the composites can hardly exhibit nonlinearity.

The chains of microvaristors in composite varistors were formed by applying an electric field during the curing process; these chains work as current paths, as shown in Figure 1.17 [123]. This kind of composite varistor shows superior nonlinear voltage–current characteristics despite small microvaristor content.

Besides good overvoltage protection effect, the polymer blended with microvaristor filler can function as field grading material (FGM) due to its excellent nonlinear J–E characteristics. It possesses field-dependent electrical parameters, and is thus widely used for stress control and field grading in all fields of electrical insulations [120, 121].

References

1 http://en.wikipedia.org/wiki/Varistor.
2 Clarke, D.R. (1999). Varistor ceramics. *Journal of the American Ceramic Society* 82 (3): 485–502.
3 Matsuoka, M. (1971). Nonohmic properties of zinc oxide ceramics. *Japanese Journal of Applied Physics* 10 (6): 736–746.

4 Levinson, L.M. and Philipp, H.R. (1986). Zinc oxide varistors-a review. *American Ceramic Society Bulletin* 65 (4): 639–646.

5 Einzinge, R. (1981). Grain boundary properties in ZnO varistors. *Advances in Ceramics* 1: 359–374.

6 Eda, K. (1989). Zinc oxide varistors. *IEEE Electrical Insulation Magazine* 5 (6): 28–30.

7 Addison, W.E. (1953). *Structural Principles in Inorganic Compounds*, 57. New York: Wiley.

8 Gupta, T.K. (1990). Application of zinc oxide varistors. *Journal of the American Ceramic Society* 73 (7): 1817–2177.

9 Zhou, Z., Kato, K., Komaki, T. et al. (2004). Effects of dopants and hydrogen on the electrical conductivity of ZnO. *Journal of the European Ceramic Society* 24 (1): 139–149.

10 Pillai, S.C., Kelly, J.M., Ramesh, R., and McCormack, D.E. (2013). Advances in the synthesis of ZnO nanomaterials for varistor devices. *Journal of Materials Chemistry C* 1 (20): 3268–3281.

11 Ziegler, E., Heinrich, A., Oppermann, H., and Stöver, G. (1982). Growth and electrical properties of non-stoichiometric ZnO single crystals doped with Co. *Physica Status Solidi (A)* 70 (2): 563–570.

12 Pillai, S.C., Kelly, J.M., McCormack, D.E., and Ramesh, R. (2008). High performance ZnO varistors prepared from nanocrystalline precursors for miniaturised electronic devices. *Journal of Materials Chemistry* 18 (33): 3926–3932.

13 He, J.L., Hu, J., and Lin, Y.H. (2008). ZnO varistors with high voltage gradient and low leakage current by doping rare-earth oxide. *Science in China, Series E, Technological Sciences* 51 (6): 693–701.

14 Daneu, N., Rečnik, A., and Bernik, S. (2011). Grain-growth phenomena in ZnO ceramics in the presence of inversion boundaries. *Journal of the American Ceramic Society* 94 (5): 1619–1626.

15 Leach, C., Ali, N.K., Cupertino, D., and Freer, R. (2010). Microwave-assisted sintering of ZnO varistors: local microstructure and functional property variations. *Materials Science and Engineering: B* 170 (1): 15–21.

16 Mazaheri, M., Zahedi, A.M., and Sadrnezhaad, S.K. (2008). Two-step sintering of nanocrystalline ZnO compacts: effect of temperature on densification and grain growth. *Journal of the American Ceramic Society* 91 (1): 56–63.

17 Dey, D. and Brad, R.C. (1992). Grain growth of ZnO during Bi_2O_3 liquid-phase sintering. *Journal of the American Ceramic Society* 75 (9): 2529–2534.

18 Gambino, J.P., Kingery, W.D., Pike, G.E. et al. (1987). Grain boundary electronic states in some simple ZnO varistors. *Journal of Applied Physics* 61 (7): 2571–2574.

19 Long, W.C., Hu, J., Liu, J., and He, J.L. (2010). Effects of cobalt doping on the electrical characteristics of Al-doped ZnO varistors. *Materials Letters* 64 (9): 1081–1084.

20 Fan, J. and Freer, R. (1993). Improvement of the non-linearity and degradation behaviour of ZnO varistors. *British Ceramic Transactions* 92 (6): 221–226.

21 Asokan, T. and Freer, R. (1990). Characterization of spinel particles in zinc oxide varistors. *Journal of Materials Science* 25 (5): 2447–2453.

22 Look, D.C. (2001). Recent advances in ZnO materials and devices. *Materials Science and Engineering: B* 80 (1): 383–387.

23 Bartkowiak, M., Mahan, G.D., Modine, F.A., and Alim, M.A. (1996). Influence of ohmic grain boundaries in ZnO varistors. *Journal of Applied Physics* 79 (1): 273–281.

24 Han, J.P.A., Senos, M.R., and Mantas, P.Q. (2002). Defect chemistry and electrical characteristics of undoped and Mn-doped ZnO. *Journal of the European Ceramic Society* 22 (1): 49–59.

25 Kutty, T.R.N. and Raghu, N. (1989). Varistors based on polycrystalline ZnO: Cu. *Applied Physics Letters* 54 (18): 1796–1798.

26 Carlsson, J.M., Hellsing, B., Domingos, H.S., and Bristowe, P.D. (2001). Electronic properties of a grain boundary in Sb-doped ZnO. *Journal of Physics: Condensed Matter* 13 (44): 9937–9943.

27 Fan, J. and Freer, R. (1993). The electrical properties and dc degradation characteristics of silver doped ZnO varistors. *Journal of Materials Science* 28 (5): 1391–1395.

28 Bernik, S. and Daneu, N. (2007). Characteristics of ZnO-based varistor ceramics doped with Al_2O_3. *Journal of the European Ceramic Society* 27 (10): 3161–3170.

29 Daneu, N., Rečnik, A., and Bernik, S. (2003). Grain growth control in Sb_2O_3-doped zinc oxide. *Journal of the American Ceramic Society* 86 (8): 1379–1384.

30 Han, J., Mantas, P.Q., and Senos, A.M.R. (2001). Densification and grain growth of Al-doped ZnO. *Journal of Materials Research* 16 (2): 459–468.

31 Gambino, J.P., Kingery, W.D., Pike, G.E. et al. (1987). Grain boundary electronic states in some simple ZnO varistors. *Journal of Applied Physics* 61 (7): 2571–2574.

32 Clarke, D.R. (1979). Grain-boundary segregation in a commercial ZnO-based varistor. *Journal of Applied Physics* 50 (11): 6829–6832.

33 Einzinger, R. (1987). Metal oxide varistors. *Annual Review of Materials Science* 17 (1): 299–321.

34 Sousa, V.C., Segadaes, A.M., Morelli, M.R., and Kiminami, R.H.G.A. (1999). Combustion synthesized ZnO powders for varistor ceramics. *International Journal of Inorganic Materials* 1 (3): 235–241.

35 Inada, M. (1980). Formation mechanism of nonohmic zinc oxide ceramics. *Japanese Journal of Applied Physics* 19 (3): 409–419.

36 Bemik, S. and Daneu, N. (2007). Characteristics of ZnO-based varistor ceramics doped with Al_2O_3. *Journal of the European Ceramic Society* 27 (10): 3161–3170.

37 Hu, J. (2008). Research of ZnO varistor with high voltage gradient applied in ultra-high voltage arrester. PhD thesis. Tsinghua University, Beijing, China.

38 Matsuoka, M., Masuyama, T., and Iida, Y. (1969). Voltage nonlinearity of zinc oxide ceramics doped with alkali-earth metal oxide. *Japanese Journal of Applied Physics* 8 (10): 1275–1276.

39 Valeyev, K.S., Knayazev, V.A., and Drozdov, N.O. (1964). Non-linear varistors using oxides of zinc, silicon and tin. *Elektrichestvo* 4: 72–76.

40 Kosman, M.S. and Pettsold, E.G. (1961). O wozmoznosti izgotowlenija simietriczeskich varistorov iz okisi cinka c primiestju okosi bizmuta. [On a possibility of manufacturing symmetric varistors from bismuth oxide dopped zinc oxide]. *Uczonyje Zapiski LGPT im. AI Gercena* 207: 191–196.

41 Levinson, L.M. (1989). *Ceramic Transactions, Vol. 3, Advances in Varistor Technology*. Westerville, OH: American Ceramic Society.

42 Kresge, J.S., Sakshaug, E.C., Fishman, H., and Ellis, H.F. (1989). A history of the development of metal oxide technology at GE for utility system surge arresters. *Ceramic Transactions* 3: 207–218.

43 Mukae, K., Tsuda, K., and Nagasawa, I. (1977). Non-ohmic properties of ZnO-rare earth metal oxide-Co_3O_4 ceramics. *Japanese Journal of Applied Physics* 16 (8): 1361–1368.

44 Mukae, K. (1987). Zinc oxide varistors with praseodymium oxide. *American Ceramic Society Bulletin* 66 (9): 1329–1331.

45 Pike, G. E. (1982). Electronic properties of ZnO-varistors: a new model. Materials Research Society Meeting, Boston, MA, USA.

46 Pike, G.E. and Seager, C.H. (1979). The dc voltage dependence of semiconductor grain-boundary resistance. *Journal of Applied Physics* 50 (5): 3414–3422.

47 Blatter, G. and Baeriswyl, D. (1987). High-field transport phenomenology: hot-electron generation at semiconductor interfaces. *Physical Review B* 36 (12): 6446–6464.

48 Blatter, G. and Greuter, F. (1986). Carrier transport through grain boundaries in semiconductors. *Physical Review B* 33 (6): 3952–3966.

49 Blatter, G. and Greuter, F. (1986). Electrical breakdown at semiconductor grain boundaries. *Physical Review B* 34 (12): 8555–8572.

50 Tao, M., Ai, B., Dorlanne, O., and Loubiere, A. (1987). Different single grain junctions within a ZnO varistor. *Journal of Applied Physics* 61 (4): 1562–1567.

51 Wang, H., Schulze, W.A., and Cordaro, J.F. (1995). Averaging effect on current-voltage characteristics of ZnO varistors. *Japanese Journal of Applied Physics* 34 (5A): 2352–2358.

52 Bartkowiak, M. and Mahan, G.D. (1995). Nonlinear currents in Voronoi networks. *Physical Review B* 51 (16): 10825–10828.

53 Sakshaug, E.C., Burke, J.J., and Kresge, J.S. (1989). Metal oxide arresters on distribution systems: fundamental considerations. *IEEE Transactions on Power Delivery* 4 (4): 2076–2089.

54 Kirkby, P., Erven, C.C., and Nigol, O. (1988). Long-term stability and energy discharge capacity of metal oxide valve elements. *IEEE Transactions on Power Delivery* 3 (4): 1656–1665.

55 Kan, M., Nishiwaki, S., Sato, T. et al. (1983). Surge discharge capability and thermal stability of a metal oxide surge arrester. *IEEE Transactions on Power Apparatus and System* 102 (2): 282–289.

56 Bartkowiak, M., Comber, M.G., and Mahan, G.D. (1999). Failure modes and energy absorption capability of ZnO varistors. *IEEE Transactions on Power Delivery* 14 (1): 152–162.

57 Ringler, K.G., Kirkby, P., Erven, C.C. et al. (1997). The energy absorption capability and time-to-failure of varistors used in station-class metal–oxide surge arresters. *IEEE Transactions on Power Delivery* 12 (1): 203–212.

58 Wang, S.L., Ga, S.X., Li, H.F., and Xu, Y.B. (1992). The relation between testing waveform and energy density on ZnO varistor. In: *Annual Report of Conference on Electrical Insulation and Dielectric Phenomena*, 543–548. IEEE.

59 He, J.L. and Hu, J. (2007). Analysis on nonuniformity of energy absorption capabilities of ZnO varistors. *IEEE Transactions on Power Delivery* 22 (3): 1523–1532.

60 Sweetana, A., Kunkle, N., Hingorani, N., and Tahiliani, V. (1982). Design, development and testing of 1200 kV and 550 kV gapless surge arresters. *IEEE Transactions on Power Apparatus and Systems* 101 (7): 2319–2327.

61 He, J.L., Cho, H.G., and Han, S.W. (1998). Impulse destruction mechanisms of ZnO varistors. *Journal of the Korean Physical Society* 11 (4): 460–467.

62 Eda, K., Iga, A., and Matsuoka, M. (1980). Degradation mechanism of non-ohmic zinc oxide ceramics. *Journal of Applied Physics* 51 (5): 2678–2684.

63 Gupta, T.K. and Carlson, W.G. (1985). A grain-boundary defect model for instability/stability of a ZnO varistor. *Journal of Materials Science* 20 (10): 3487–3500.

64 Liu, J. (2011). Research on the degradation characteristics and mechanisms of high voltage gradient ZnO varistor. PhD thesis. Tsinghua University, Beijing.

65 Chisholm, W.A. (2010). New challenges in lightning impulse flashover modeling of air gaps and insulators. *IEEE Electrical Insulation Magazine* 26 (2): 14–25.

66 Frosch, C.J. (1954). Improved silicon carbide varistors. *Bell Laboratory Records* 32: 336–340.

67 Dienel, H.F. (1956). Silicon carbide varistors: properties and construction. *Bell Laboratory Records* 34: 407–411.

68 Masuyama, T. and Matsuoka, M. (1968). Current dependence of voltage non-linearity in SiC varistors. *Japanese Journal of Applied Physics* 7 (10): 1294.

69 He, J.L., Li, C., Hu, J., and Zeng, R. (2011). Deep suppression of switching overvoltages in AC UHV systems using low residual arresters. *IEEE Transactions on Power Delivery* 26 (4): 2718–2725.

70 Furukawa, S., Usuda, O., Isozaki, T., and Irie, T. (1999). Development and application of lightning arresters for transmission lines. *IEEE Transactions on Power Delivery* 4 (4): 2121–2129.

71 Koch, R.E., Timoshenko, J.A., Anderson, J.G., and Shih, C.H. (1985). Design of zinc oxide transmission line arresters for application on 138 kV towers. *IEEE T Transactions Power Apparatus and System* 104 (10): 2675–2680.

72 He, J.L., Zeng, R., Chen, S.M., and Tu, Y.P. (2003). Thermal characteristics of high voltage whole-solid-insulated polymeric ZnO surge arrester. *IEEE Transactions on Power Delivery* 18 (3): 1221–1227.

73 Tarasiewicz, E.J., Rimmer, F., and Morched, A.S. (2004). Transmission line arrester energy, cost, and risk of failure analysis for partially shielded transmission lines. *IEEE Transactions on Power Delivery* 15 (3): 919–924.

74 Sadovic, S., Joulie, R., Tartier, S., and Brocard, E. (1997). Use of line surge arresters for the improvement of the lightning performance of 63 kV and 90 kV shielded and unshielded transmission lines. *IEEE Transactions on Power Delivery* 12 (3): 1232–1240.

75 Ishida, K., Dokai, K., Tsozaki, T. et al. (1992). Development of a 500 kV transmission line arrester and its characteristics. *IEEE Transactions on Power Delivery* 7 (3): 1265–1274.

76 Yamada, T., Sawada, J., Zaima, E. et al. (1993). Development of suspension-type arresters for transmission lines. *IEEE Transactions on Power Delivery* 8 (3): 1052–1060.

77 He, J.L., Chen, S.M., Zeng, R. et al. (2006). Development of polymeric surge ZnO arresters for 500-kV compact transmission line. *IEEE Transactions on Power Delivery* 21 (1): 113–120.

78 Mukae, K., Tsuda, K., and Nagasawa, I. (1977). Non-ohmic properties of ZnO-rare earth metal oxide-Co_3O_4 ceramics. *Japanese Journal of Applied Physics* 16 (8): 1361–1368.

79 Nahm, C.H. (2012). Sintering effect on ageing behavior of rare earths (Pr_6O_{11}-Er_2O_3-Y_2O_3)-doped ZnO varistor ceramics. *Journal of Rare Earths* 30 (10): 1028–1032.

80 Fan, J. and Freer, R. (1997). Varistor properties and microstructure of ZnO–BaO ceramics. *Journal of Materials Science* 32 (2): 415–419.

81 Tsai, J.K. and Wu, T.B. (1994). Non-ohmic characteristics of ZnO-V_2O_5 ceramics. *Journal of Applied Physics* 76 (8): 4817–4822.

82 Franken, P.E.C., Viegers, M.P.A., and Gehring, A.P. (1981). Microstructure of $SrTiO_3$ boundary-layer capacitor material. *Journal of the American Ceramic Society* 64 (12): 687–690.

83 Yan, M.F. and Rhodes, W.W. (1982). Preparation and properties of TiO_2 varistors. *Applied Physics Letters* 40 (6): 536–537.

84 Subramanian, M.A., Li, D., Duan, N. et al. (2000). High dielectric constant in $ACu_3Ti_4O_{12}$ and $ACu_3Ti_3FeO_{12}$ phases. *Journal of Solid State Chemistry* 151: 323–325.

85 Li, J., Subramanian, M.A., Rosenfeld, H.D. et al. (2004). Clues to the giant dielectric constant of $CaCu_3Ti_4O_{12}$ in the defect structure of "$SrCu_3Ti_4O_{12}$". *Chemistry of Materials* 16 (25): 5223–5225.

86 Ramirez, A.P., Subramanian, M.A., Gardel, M. et al. (2000). Giant dielectric constant response in a copper-titanate. *Solid State Communications* 115 (5): 217–220.

87 Chung, S.Y., Kim, I.D., and Kang, S.J. (2004). Strong nonlinear current–voltage behaviour in perovskite-derivative calcium copper titanate. *Nature Materials* 3: 774–778.

88 Chen, Y.L. and Yang, S.F. (2011). PTCR effect in donor doped barium titanate: review of compositions, microstructures, processing and properties. *Advances in Applied Ceramics* 110 (5): 257–269.

89 Pianaro, S.A., Bueno, P.R., Longo, E., and Varela, J.A. (1995). A new SnO_2-based varistor system. *Journal of Materials Science Letters* 14 (10): 692–694.

90 Leite, E.R., Nascimento, A.M., Bueno, P.R. et al. (1999). The influence of sintering process and atmosphere on the non-ohmic properties of SnO_2 based varistor. *Journal of Materials Science: Materials in Electronics* 10 (4): 321–327.

91 Pianaro, S.A., Bueno, P.R., Olivi, P. et al. (1997). Effect of Bi_2O_3 addition on the microstructure and electrical properties of the SnO_2-CoO-Nb_2O_5 varistor system. *Journal of Materials Science Letters* 16 (8): 634–638.

92 Pianaro, S.A., Bueno, P.R., Olivi, P. et al. (1998). Electrical properties of the SnO_2-based varistor. *Journal of Materials Science: Materials in Electronics* 9 (2): 159–165.

93 Pianaro, S.A., Bueno, P.R., Longo, E., and Varela, J.A. (1999). Microstructure and electric properties of a SnO_2 based varistor. *Ceramics International* 25 (1): 1–6.

94 Bueno, P.R., Cassia-Santos, M.R., Leite, E.R. et al. (2000). Nature of the Schottky-type barrier of highly dense SnO_2 systems displaying nonohmic behavior. *Journal of Applied Physics* 88 (11): 6545–6548.

95 Bueno, P.R., Leite, E.R., Oliveira, M.M. et al. (2001). Role of oxygen at the grain boundary of metal oxide varistors: a potential barrier formation mechanism. *Applied Physics Letters* 79 (1): 48–50.

96 Makarov, V. and Trontelj, M. (1994). Novel varistor material based on tungsten oxide. *Journal of Materials Science Letters* 13 (13): 937–939.

97 Filho, A.G.S., Matias, J.G.N., Dias, N.L. et al. (1999). Microstructural and electrical properties of sintered tungsten trioxide. *Journal of Materials Science* 34 (5): 1031–1035.

98 Wang, Y., Yao, K.L., and Liu, Z.L. (2001). Novel nonlinear current-voltage characteristics of sintered tungsten oxide. *Journal of Materials Science Letters* 20 (18): 1741–1743.

99 Li, T.Y., Wang, H.Q., Hua, Z.Q. et al. (2010). Densification and grain growth of CuO-doped Pr_6O_{11} varistors. *Ceramics International* 36 (5): 1511–1516.

100 Philip, J. and Kutty, T.R.N. (2001). Nonlinear current–voltage relations in polycrystalline perovskite manganites ceramics. *Applied Physics Letters* 79 (2): 209–211.

101 Li, T.Y., Zhao, H.W., Dong, L. et al. (2008). Novel varistor material based on terbium oxide. *Journal of Physics D: Applied Physics* 42 (3): 035401.

102 Rossinelli, M., Greuter, F., and Schmuckle, F. (1989). Electrically active grain boundaries in ceramics: varistors and capacitors in electroceramics. *British Ceramic Proceedings* 41: 177–188.

103 Pavlov, A.N. and Raevski, I.P. (1997). Varistor effect in semiconductor ferroelectrics. *Technical Physics* 42 (12): 1390–1394.

104 Glatz-Reichenbach, J., Meyer, B., Strümpler, R. et al. (1996). New low-voltage varistor composites. *Journal of Materials Science* 31 (22): 5941–5944.

105 Yang, X., Kim, H., Yang, L. et al. (2014). Composite varistors based on epoxy resin/$La_{0.8}Sr_{0.2}MnO_3$. *Journal of Composite Materials* 48 (6): 677–681.

106 Hashimov, A.M., Hasanli, S.M., Mehtizadeh, R.N. et al. (2006). Zinc oxide-and polymer-based composite varistors. *Physica Status Solidi (C)* 3 (8): 2871–2875.

107 Lin, C.C., Lee, W.S., Sun, C.C., and Whu, W.H. (2008). A varistor–polymer composite with nonlinear electrical-thermal switching properties. *Ceramics International* 34 (1): 131–136.

108 Modine, F.A. and Hyatt, H.M. (1988). New varistor material. *Journal of Applied Physics* 64 (8): 4229–4232.

109 Wang, Z., Nelson, J.K., Hillborg, H. et al. (2012). Graphene oxide filled nanocomposite with novel electrical and dielectric properties. *Advanced Materials* 24 (23): 3134–3137.

110 Mårtensson, E. and Gäfvert, U. (2003). Three-dimensional impedance networks for modelling frequency dependent electrical properties of composite materials. *Journal of Physics D: Applied Physics* 36 (15): 1864–1872.

111 Bidadi, H., Aref, S.M., Ghafouri, M. et al. (2013). Effect of changing gallium arsenide content on gallium arsenide–polymer composite varistors. *Journal of Physics and Chemistry of Solids* 74 (8): 1169–1173.

112 Bidadi, H., Aref, S.M., Ghafouri, M. et al. (2013). The effect of sintering temperature on varistor characteristics of gallium arsenide–polyaniline–polyethylene composite varistors. *Materials Science in Semiconductor Processing* 16 (3): 752–758.

113 Aref, S.M., Olad, A., Parhizkar, M. et al. (2013). Effect of polyaniline content on electrophysical properties of gallium arsenide–polymer composite varistors. *Solid State Sciences* 26: 128–133.

114 Anas, S., Mahesh, K.V., Jeen Maria, M., and Ananthakumar, S. (2017). Sol-gel materials for varistor devices. In: *Sol-Gel Materials for Energy, Environment and Electronic Applications*, 23–59. Springer International Publishing.

115 Ghafouri, M., Parhizkar, M., Aref, S.M. et al. (2014). Effect of temperature on the electrophysical properties of Si–polymer composite varistors. *Microelectronics Reliability* 54 (5): 965–971.

116 Ghafouri, M., Parhizkar, M., Bidadi, H. et al. (2014). Effect of Si content on electrophysical properties of Si–polymer composite varistors. *Materials Chemistry and Physics* 147 (3): 1117–1122.

117 Yang, X., Hu, J., Chen, S.M., and He, J.L. (2016). Understanding the percolation characteristics of nonlinear composite dielectrics. *Scientific Reports* 6: 30597.

118 Yang, X., He, J.L., and Hu, J. (2015, 2015). Tailoring the nonlinear conducting behavior of silicone composites by ZnO microvaristor fillers. *Journal of Applied Polymer Science* 132 (40): 42645.

119 Gao, L., Yang, X., Hu, J., and He, J.L. (2016). ZnO microvaristors doped polymer composites with electrical field dependent nonlinear conductive and dielectric characteristics. *Materials Letters* 171: 1–4.

120 Zhao, X.L., Yang, X., Li, Q. et al. (2017). Synergistic effect of ZnO microspherical varistors and carbon fibers on nonlinear conductivity and mechanical properties of the silicone rubber-based material. *Composites Science and Technology* 150: 187–193.

121 Dang, Z.M., Yuan, J.K., Zha, J.W. et al. (2012). Fundamentals, processes and applications of high-permittivity polymer–matrix composites. *Progress in Materials Science* 57 (4): 660–723.

122 Simon, P. and Gogotsi, Y. (2008). Materials for electrochemical capacitors. *Nature Materials* 7 (11): 845–854.

123 Ishibe, S., Mori, M., Kozako, M., and Hikita, M. (2014). A new concept varistor with epoxy/microvaristor composite. *IEEE Transactions on Power Delivery* 29 (2): 677–682.